ISBN: 978-3-95450-214-1 ISSN: 2673-5490 doi:10.18429/JACoW-IPAC2021-WEPAB165

METAMATERIAL WAVEGUIDE HOM LOADS FOR SRF ACCELERATING CAVITIES

S. Kuzikov†, Euclid Techlabs LLC, Bolingbrook, IL, USA

Abstract

Suppression of beam induced HOMs is necessary for most SRF accelerating cavities driven with high currents. One of the problems in design of a HOM load is that vacuum compatible materials with high enough imaginary part of the dielectric permittivity, which provides absorption, have also a high real part of the permittivity. This does not allow absorbing RF radiation at short distance and in broad frequency band. We propose considering artificial metamaterials where besides lossy dielectric pieces, an absorber with high magnetic permeability is included. In our proposal, we suggest composing a waveguide HOM load of a metamaterial consisted of well-known ceramic and ferrite plates placed periodically in a stack. Such a design provides low return losses, compactness and broad frequency range of the operation.

METAMATERIAL WAVEGUIDE LOAD CONCEPT

There is a well-known and fundamental solution of Maxwell's equations in which a plane electromagnetic wave penetrates through the boundary between a vacuum and a material surface without reflection. In this solution, for normal plane wave incidence, the dielectric permittivity and magnetic permeability of the material must be equal to each other. Note that the mentioned ε and μ can be arbitrary complex numbers. Thus far, such "ideal" materials are unknown. In order to remove this block, we suggest considering artificial metamaterials, where in addition to the lossy dielectric portion, an absorber with high magnetic permeability is also included. In our proposal, we suggest composing a waveguide HOM load from a metamaterial consisting of well-known ceramic and ferrite plates placed periodically in a stack. The period must be small compared to the wavelength of the electromagnetic wave. Each plate is non-resonant, and ε and μ have only a slowly varying dependence on frequency. Such a design should provide low reflection, compactness, and also a broad frequency range of operation. Because an SRF cavity is sensitive to magnetic fields at the mG level, we propose the use of ferrite-containing metamaterials for a waveguide load only when it is located far from the SRF cavity itself. In this case, the ferrites, which potentially could become magnetized, will not affect the niobium cavity.

Main Equations

Let us consider the reflection and refraction of a plane wave by a boundary between vacuum and a medium having some complex permittivity and permeability (Fig. 1). In the case of the so-called parallel polarization (Fig. 1a), the reflection coefficient is given by the equation [1]:

$$R_{par} = \frac{cos\varphi - \sqrt{\frac{\mu}{\varepsilon}}cos\psi}{cos\varphi + \sqrt{\frac{\mu}{\varepsilon}}cos\psi}, \quad (1)$$

where φ is the angle of incidence and ψ - is an angle of refraction given by:

$$\frac{sin\varphi}{sin\psi} = \sqrt{\varepsilon\mu}. \quad (2)$$

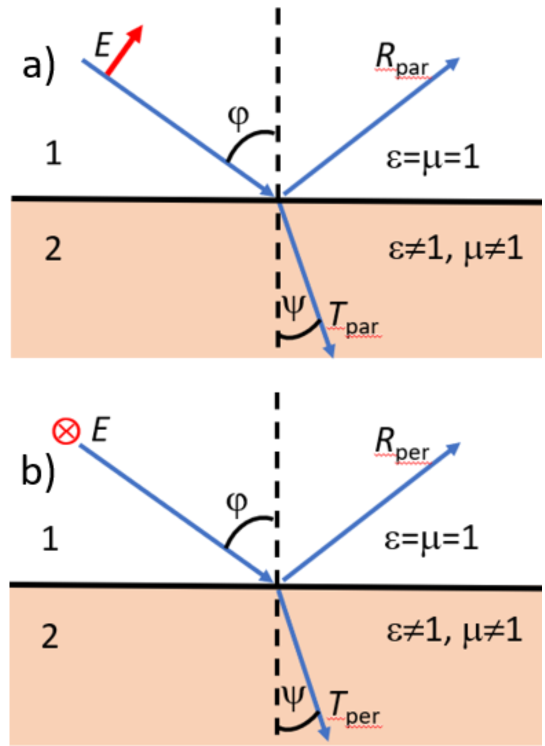

Figure 1: Plane wave reflection and transmission diagram for parallel (a) and perpendicular (b) polarizations.

The numerator of the Eq. (1) equals zero if the following condition is satisfied:

$$\mu = \frac{\varepsilon^2 cos^2\varphi + sin^2\varphi}{\varepsilon}. \quad (3)$$

For the case of |ε|>>1, which is true for most ceramics, Eq. (2) takes a remarkably simple form:

$$\frac{\mu}{\varepsilon} = cos^2\varphi. \quad (4)$$

Because both ε and μ are assumed to have complex values, instead of (4) one can write two separate conditions that together are equivalent to Eq. (4):

$$\frac{\mu'}{\varepsilon'} = cos^2\varphi, \quad (5)$$

$$tan\delta_\varepsilon = tan\delta_\mu \quad (6)$$

where $tan\delta_\varepsilon = \varepsilon''/\varepsilon'$ - is the electrical loss tangent and $tan\delta_\mu = \mu''/\mu'$ - is the magnetic loss tangent.

† s.kuzikov@euclidtechlabs.com

ISBN: 978-3-95450-214-1 ISSN: 2673-5490 doi:10.18429/JACoW-IPAC2021-WEPAB165

Note that the obtained conditions (4) or (5) and (6) do not depend on frequency, i.e., they promise an extremely broadband reflectionless regime. The bandwidth would be determined by the cut-off frequency in a waveguide and by the direct dependence of ε and μ on frequency.

The case of the perpendicular polarization (Fig. 1b) is analyzed in a similar way, and the result is that the reflection coefficient is given by the equation:

$$R_{per} = \frac{\sqrt{\frac{\mu}{\varepsilon}}cos\varphi - cos\psi}{\sqrt{\frac{\mu}{\varepsilon}}cos\varphi + cos\psi}, \quad (7)$$

and the result is that one needs to satisfy a condition which is similar to the one obtained in the Eq. (4):

$$\frac{\varepsilon}{\mu} = cos^2\varphi. \quad (8)$$

MODELING AND SIMULATIONS

The Eqs. (5) say that the perfectly matched transmission of an RF wave is possible at some angle (5) for a lossy media with arbitrary large ε′ and μ′. But an additional condition also needs to be satisfied, which is that the electric and magnetic loss tangents must be equal to each other in accordance with (6). If there is a material with the necessary values of ε and μ, and if we assume that the fundamental TE_{10} mode is far from cut off, a HOM load can be designed either as a slab (Fig. 2a) or as a pair of slabs (Fig. 2b) located in a waveguide. The second configuration allows one to double load height in comparison with the configuration shown in the Fig. 2a. The slabs must be inclined at the angle α=π/2-φ with respect to the waveguide axis.

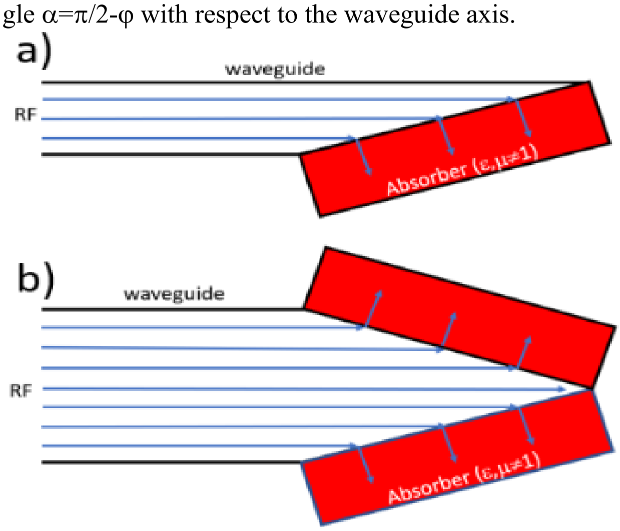

Figure 2: Configurations of waveguide HOM loads.

Let us show how the described idea works by means of an example using an existing ferrite. In [2], the sulfide-based nanomaterial (MoS_2@FeCo) is considered. It has ε′=7.9, $tan\delta_\varepsilon$=0.26, μ′=0.95, and $tan\delta_\mu$=0.25 when measured at 14.4 GHz. In accordance with Eqs. (5) and (6), this material will provide good matching at the angle φ=69.7°.

Figure 3 shows the simulated S_{11} parameter for a load based on WR90 waveguide configured as in Fig. 2a. The reflection is less than -20 dB over an extremely broad frequency band. The reflection does go up, of course, when the frequency approaches cut off (the left side of the dependence on frequency shown in the Fig. 3). The field structure (Fig. 4) is shown at the frequency 14.4 GHz at which the parameters of this material were measured [2].

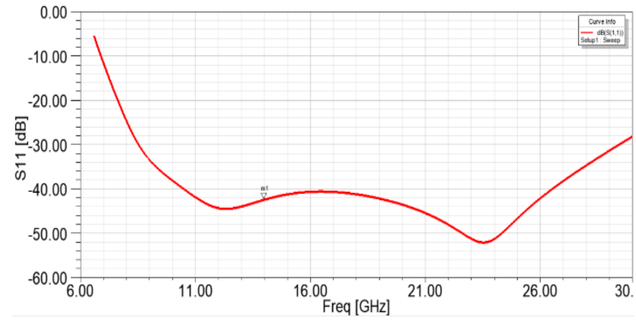

Figure 3: S_{11} (return loss) parameter vs frequency for sulfide-based ferrite load.

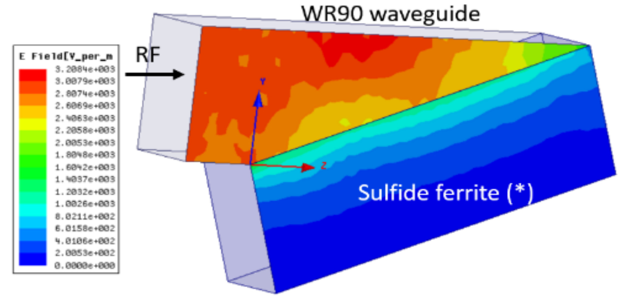

Figure 4: Field structure for a sulfide-based ferrite load.

Composition of a Metamaterial Reflectionless Media

The next step in creating a new material with the necessary properties is to combine several sub-materials in a common volume. In this case, the average ε and μ of an artificial material consisting of several other sub-components can be written based on the natural assumption that each sub-component material contributes to the real and imaginary parts of ε and μ in proportion to its own volumetric fraction:

$$< \varepsilon' \geq \sum_i v_i \varepsilon_i', \quad < \varepsilon'' \geq \sum_i v_i \varepsilon_i'', \quad (8)$$
$$< \mu' \geq \sum_i v_i \mu_i', \quad < \mu'' \geq \sum_i v_i \mu_i'', \quad (9)$$

where v_i – is the fractional content of the i^th subcomponent material, and $\sum_i v_i = 1$.

Table 1: Metamaterial Absorber Parameters for Matching Angle 75.1°

Component	**ε′**	**$tan\delta_\varepsilon$**	**μ′**	**$tan\delta_\mu$**	**Percentage**
Ceralloy	28	0.2	1	0	49%
HexMZ	18	0.039	2	0.25	40%
Vacuum	1	0	1	0	11%

ISBN: 978-3-95450-214-1 ISSN: 2673-5490 doi:10.18429/JACoW-IPAC2021-WEPAB165

Now let us consider how to compose a reflectionless metamaterial from real existing ceramics and ferrites that are already used for HOM loads. The third natural sub-component to be considered is the vacuum (ε=μ=1). Tables of ceramics parameters can be found in [3], and three types of ferrites are well described in [4]. Using the Eqs. (8) and (9) and the conditions (5) and (6), one can easily generate several appealing material combinations. For example, one metamaterial combination is represented at the Table 1.

This case was used to simulate a load (Fig. 5) based on a 105×22.5 mm^2 cross-section waveguide. If we chose the configuration in Fig. 2b, the load would have 105×50 mm^2 cross-section as in [5]. The absorbing material was composed of a periodic stack of the plates with a period of 12 mm, a width of 105 mm, and a height of 27 mm. The thickness of the Ceralloy plates was taken as 6 mm, the thickness of the ferrite was taken as 5 mm, and there were 1-mm vacuum gaps between pairs of these plates (see Fig. 5). The total load length was 92 mm. The S_{11} parameter for the fundamental TE_{10} mode is plotted in Fig. 6. Figure 7 shows the S-parameters of higher order modes propagated to the load. This information about higher-order modes is important, because spatial structures of HOMs cannot be known in advance. For our HOM load sizes the nearest propagating modes to the fundamental TE_{10} mode are TE_{20}, TE_{30} and TE_{40}. The field structure, shown in Fig. 8, corresponds to the frequency of 2 GHz.

For the mentioned simulations shown in the Figs. 6 and 7, we used frequency-dependent values of ε and μ for both types of the plates. The information was taken from [3] and [4]. Three points were taken for the ceramics and ferrites, at 1 GHz, 8 GHz, and 10 GHz. Between these points, the real and imaginary parts of ε and μ were calculated in accordance with linear approximations. From these simulations, one can conclude that the load shows low return loss over a broad frequency band.

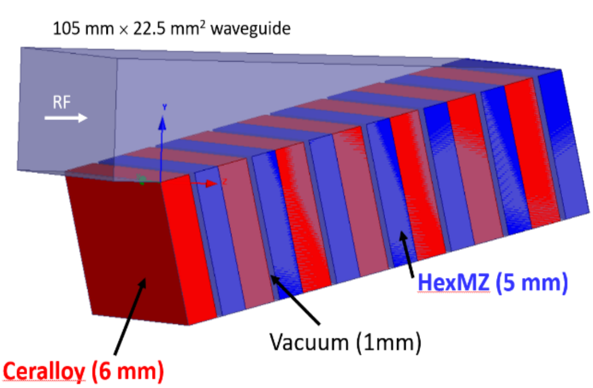

Figure 5: Metamaterial load composed of Ceralloy plates (red), HexMZ ferrite plates (blue) and vacuum gaps between these plates. Only one half of the geometry is shown.

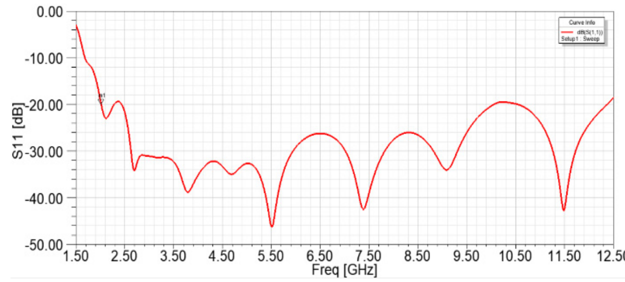

Figure 6: S_{11}-parameter (TE_{10} return loss) vs frequency for a metamaterial load composed of Ceralloy and HexMZ plates, as well as vacuum gaps, with a realistic frequency-dependent ε and μ for both sub-materials.

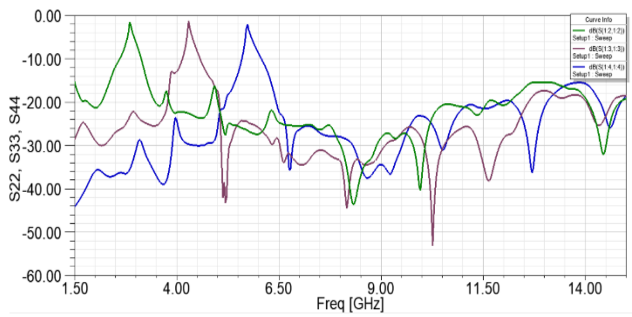

Figure 7: TE_{20} (green), TE_{30} (brown) and TE_{40} (blue) return losses.

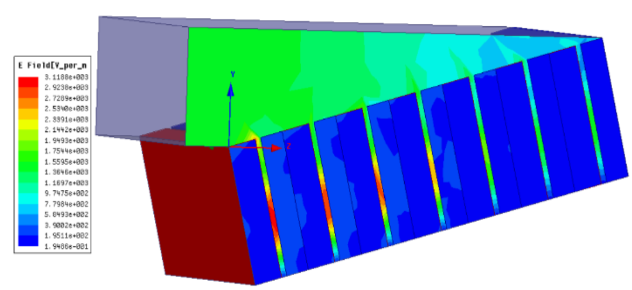

Figure 8: The field structure in the metamaterial load at frequency of 2 GHz.

The simulation results shown in Fig. 6 and 7 allow us to compare the proposed load with a similar load, the bERLinPro HOM load (JLAB and HZB), whose parameters were published in [5]. One can see that the proposed load has less reflection comparing to bERLinPro HOM load, the bandwidth is at least 1.5 times higher, and length is twice less.

CONCLUSION

New compact broadband HOM loads are proposed. They are assembled as a stack of ultrahigh vacuum compatible ceramic and ferrite plates, which are placed in a periodic order in a rectangular cross-section waveguide. In order to satisfy the best matching for the boundary between vacuum and the metamaterial, the parameters of this metamaterial, ε and μ, can be controlled by changing the content (percentage) of the mentioned sub-materials.

ISBN: 978-3-95450-214-1 ISSN: 2673-5490 doi:10.18429/JACoW-IPAC2021-WEPAB165

REFERENCES

[1] L. D. Landau, E. M. Lifshitz, and L. P. Pitaevskii. *Electrodynamics of Continuous Media (2nd ed.),* vol. 8, Butterworth-Heinemann: 1984.

[2] M. Green and X. Chen, "Recent progress of nanomaterials for microwave absorption," *Journal of Materiomics*, vol. 5, no. 4, pp. 503–541, Dec. 2019.
doi:10.1016/j.jmat.2019.07.003

[3] F. Marhauser, T. S. Elliott, A. T. Wu, E. P. Chojnacki, and E. Savrun, "Absorber Materials at Room and Cryogenic Temperatures", in *Proc. 2nd Int. Particle Accelerator Conf. (IPAC'11)*, San Sebastian, Spain, Sep. 2011, paper TUPS106, pp. 1792-1794.

[4] V. Shemelin, M. Liepe, and H. Padamsee, "Characterization of ferrites at low temperature and high frequency," *Nuclear Instruments and Methods in Physics Research Section A: Accelerators, Spectrometers, Detectors and Associated Equipment*, vol. 557, no. 1, pp. 268–271, Feb. 2006. doi:10.1016/j.nima.2005.10.081

[5] J. Guo *et al.*, "Development of Waveguide HOM Loads for BERLinPro and BESSY-VSR SRF Cavities", in *Proc. 8th Int. Particle Accelerator Conf. (IPAC'17)*, Copenhagen, Denmark, May 2017, pp. 1160-1163.
doi:10.18429/JACoW-IPAC2017-MOPVA130